

LETTER TO THE EDITOR

Correlated optical, X-ray, and γ -ray flaring activity seen with *INTEGRAL* during the 2015 outburst of V404 Cygni

J. Rodriguez¹, M. Cadolle Bel², J. Alfonso-Garzón³, T. Siegert⁴, X.-L. Zhang⁴, V. Grinberg⁵, V. Savchenko⁶, J. A. Tomsick⁷, J. Chenevez⁸, M. Clavel¹, S. Corbel¹, R. Diehl⁴, A. Domingo³, C. Gouiffès¹, J. Greiner⁴, M. G. H. Krause^{9,4}, P. Laurent⁶, A. Loh¹, S. Markoff¹⁰, J. M. Mas-Hesse³, J. C. A. Miller-Jones¹¹, D. M. Russell¹², and J. Wilms¹³

¹ Laboratoire AIM, UMR 7158, CEA/CNRS/Université Paris Diderot, CEA DSM/IRFU/SAP, F-91191 Gif-sur-Yvette, France

² Max Planck Computing and Data Facility, D-85748 Garching, Germany

³ Centro de Astrobiología (CSIC-INTA), ESAC Campus, POB 78, E-28691 Villanueva de la Cañada, Spain

⁴ Max Planck Institut für extraterrestrische Physik, D-85748 Garching, Germany

⁵ Massachusetts Institute of Technology, Kavli Institute for Astrophysics and Space Research, Cambridge, MA 02139, USA

⁶ Laboratoire APC, UMR 7164, CEA/CNRS/Université Paris Diderot, Paris, France

⁷ Space Science Lab, University of California, Berkeley, CA 94720, USA

⁸ DTU Space – National Space Institute, Technical University of Denmark, Elektrovej 327-328, 2800 Lyngby, Denmark

⁹ Universitäts-Sternwarte Muenchen, Ludwig-Maximilians-Universität, Scheinerstr. 1, D-81679 Muenchen, Germany

¹⁰ Anton Pannekoek Institute for Astronomy, University of Amsterdam, P.O. Box 94249, 1090 GE Amsterdam, the Netherlands

¹¹ International Centre for Radio Astronomy Research, Curtin University, GPO Box U1987, Perth, WA 6845, Australia

¹² New York University Abu Dhabi, PO Box 129188, Abu Dhabi, United Arab Emirates

¹³ Dr. K. Reemis-Sternwarte & Erlangen Centre for Astroparticle Physics, Universität Erlangen-Nürnberg, Sternwartstr. 7, D-96049 Bamberg, Germany

ABSTRACT

After 25 years of quiescence, the microquasar V404 Cyg entered a new period of activity in June 2015. This X-ray source is known to undergo extremely bright and variable outbursts seen at all wavelengths. It is therefore an object of prime interest to understand the accretion-ejection connections. These can, however, only be probed through simultaneous observations at several wavelengths. We made use of the *INTEGRAL* instruments to obtain long, almost uninterrupted observations from 2015 June 20th, 15:50 UTC to June 25th, 4:05 UTC, from the optical V-band, up to the soft γ -rays. V404 Cyg was extremely variable in all bands, with the detection of 18 flares with fluxes exceeding 6 Crab (20–40 keV) within 3 days. The flare recurrence can be as short as ~ 20 min from peak to peak. A model-independent analysis shows that the >6 Crab flares have a hard spectrum. A simple 10–400 keV spectral analysis of the off-flare and flare periods shows that the variation in intensity is likely to be due to variations of a cut-off power law component only. The optical flares seem to be at least of two different types: one occurring in simultaneity with the X-ray flares, the other showing a delay greater than 10 min. The former could be associated with X-ray reprocessing by either an accretion disk or the companion star. We suggest that the latter are associated with plasma ejections that have also been seen in radio.

Key words. Accretion, accretion discs; X-rays: binaries; Radio continuum: stars, Stars: black holes, Stars: individuals: V404

1. Introduction

V404 Cyg (hereafter V404) is a low mass X-ray binary (LMXB) consisting of a black hole (BH) with mass estimates ranging from ~ 9 to $15 M_{\odot}$, and a $0.7^{+0.3}_{-0.2} M_{\odot}$ K3 III companion (Casares & Charles 1994; Shahbaz et al. 1994; Khargharia et al. 2010), located at a parallax distance 2.39 ± 0.14 kpc (Miller-Jones et al. 2009). The inclination of the binary's rotational axis is 67^{+3}_{-1} (Shahbaz et al. 1994; Khargharia et al. 2010), the orbital period 6.5 d (Casares et al. 1992). This transient underwent three periods of outbursts during the 20th century (Richter 1989), the last, in May 1989, leading to its discovery as an X-ray transient by the Ginga satellite (as GS 2023+338, Makino et al. 1989). V404 showed bright X-ray flares on short time scales (e.g. Makino et al. 1989; Terada et al. 1994), and this makes it an excellent source to study the connections between the accretion and ejection phenomena, which are the probable origin of this behavior. V404 is one of the closest stellar-mass BHs, making it a rare

case where quiescence could be studied in detail, and variable remnant activity, attributed to a compact jet, was detected from radio to hard X-rays (e.g. Hynes et al. 2004; Xie et al. 2014). V404 is one of the few sources that defines the radio/X-ray correlation over a large range of luminosities, down into quiescence (Corbel et al. 2008). The good knowledge of the quiescent state makes understanding new outburst observations paramount as they allow the mechanisms responsible for the increased activity to be probed.

On 2015 June 15 (MJD 57188), V404 went into outburst again. It was first detected by *Swift* (BAT and XRT) (Barthelmy et al. 2015), and then with *MAXI*, and *INTEGRAL* (Negoro et al. 2015; Kuulkers et al. 2015). These early alerts triggered follow-up observations at all wavelengths. Preliminary results all report the detection of the source, variations of specific spectral features, and an extreme flaring activity at all wavelengths (e.g. Mooley et al. 2015; Munoz-Darias et al. 2015; Ferrigno et al. 2015; Motta et al. 2015; Tetarenko et al. 2015a,b; Tsubono et al. 2015). We triggered our *INTEGRAL* ToO program to obtain

Send offprint requests to: J. Rodriguez: jrodriguez@cea.fr

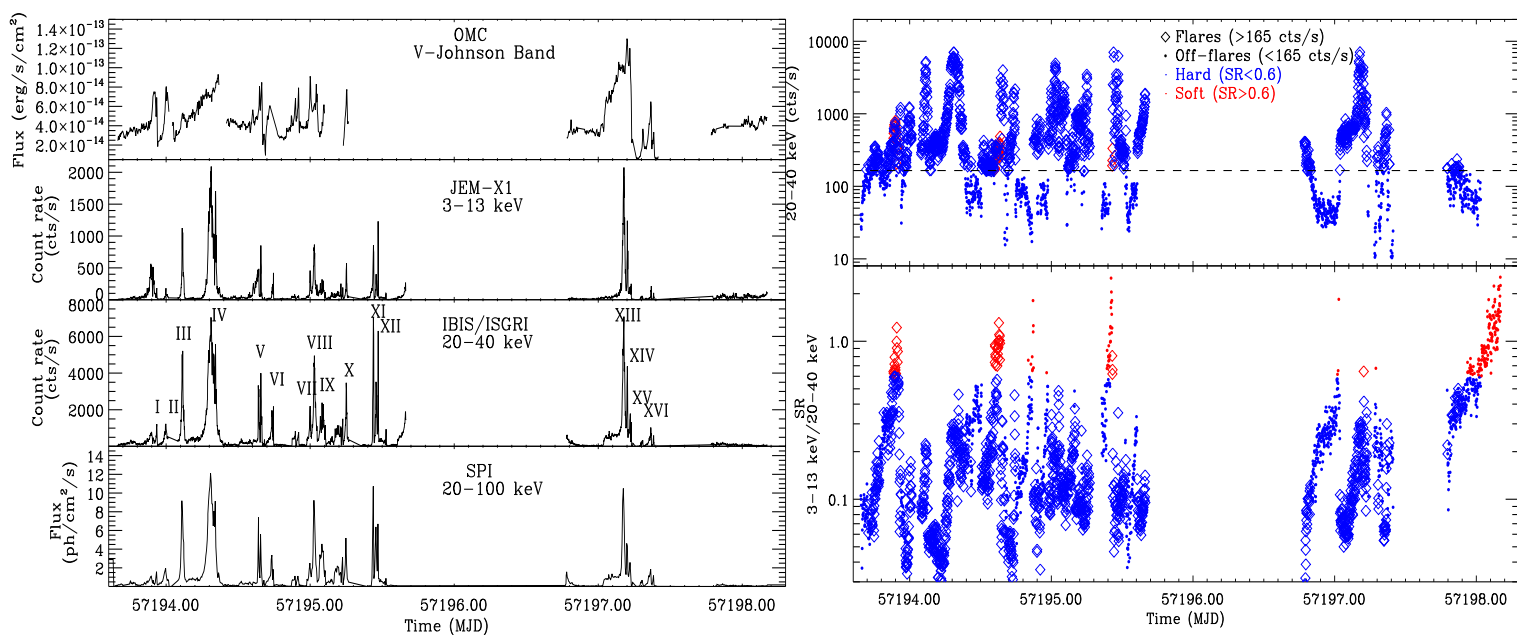


Fig. 1. **Left:** *INTEGRAL* LCs of V404 in four spectral domains (a larger version of the plot including all energy ranges is available as online material). **Right:** 20–40 keV count rate (top), and 3–13/20–40 keV softness ratio (SR, bottom). The dashed horizontal line corresponds to 1 Crab (20–40 keV). MJD 57193 is 2015 June 20th.

quasi-continuous coverage in X/ γ -rays and in the optical V band. The first detection of multiple flares exceeding 30 Crab in 20–40 keV, and possible correlated flaring in the V-band were reported in Rodriguez et al. (2015a), and Domingo et al. (2015).

Our observations caught the source during the most intense and variable phase of this new outburst. Here, we first give the details of the observations and data reduction (Sec. 2). We then focus on the flaring behavior at high energies (Sec. 3) that we compare to the activity in the optical V-band (Sec. 4). A preliminary phenomenological spectral characterization of different intensity intervals is presented in Sec. 5. We discuss our results and compare V404 to other microquasars in Sec. 6.

2. Observations and Data Reduction

Our ToO program (Fig. 1) covered MJD 57193.66–57198.17 (2015-06-20 15:50 UTC to 2015-06-25 4:05 UTC), i.e., *INTEGRAL* revolutions #1555 (continuous coverage) and #1556 (two periods). The data of all the *INTEGRAL* instruments (see Winkler et al. 2003, and references therein for all instrumental details) were reduced with the *Off line Scientific Analysis* (OSA) v10.1 software suite, with the latest calibration files available at the time of writing.

Images and 100 s binned light curves (LC) from the Joint European X-ray Monitors (JEM-X) and the Imager on Board the *INTEGRAL* Satellite (IBIS) were produced in two bands (3–13, and 13–30 keV) for JEM-X unit 1, and in four bands (20–40, 40–80, 80–150, and 150–300 keV) for the IBIS Soft Gamma-Ray Imager (ISGRI).

The event data of the Spectrometer on *INTEGRAL* (SPI) have been fitted with models for the celestial sources and instrumental background following standard reduction processes. The 20–100 keV LC of V404 as well as the other sources in the field were obtained in bins of 400 s. Background models have been built based on the pre-flaring data of a representative empty sky region, adjusting the normalization coefficient per hour (see, e.g., Strong et al. 2005, for a more general description of the method).

As source intensity and hardness vary strongly on short time scales, we extracted luminosity/hardness dependent JEM-X, ISGRI, and SPI spectra over specific time intervals of clean data. The spectra from the same time intervals were jointly fitted within XSPEC v12.8.2. Since the instruments’ responses are possibly different for the high intensities observed, only phenomenological spectral fits are presented and the fit results should be viewed with some caution.

The *INTEGRAL*/optical Monitoring Camera (OMC) fluxes and magnitudes were derived from a photometric aperture of 3×3 pixels (1 pix. = $17.504''$), slightly circularized, i.e. removing one quarter pixel from each corner (standard output from OSA). The photometric aperture was centered on the source coordinates (default centroid algorithm) and did not include any significant contribution from other objects. We removed measurements with a severe problem flag, and, to restrict the noise, only measurements of 50 and 200 s duration were considered.

3. Model independent description of the flaring

Multi-wavelength LCs of V404 from the V band up to γ -rays are highly structured with several large flares separated by calmer periods seen in all bands (Fig. 1, and see also Fig. 4 for a plot with all energy ranges). In the following, count rates (CR) are given in the ISGRI 20–40 keV range. When the source CR increased above ~ 150 – 200 cts/s an intense X-ray flare systematically followed. In the following, we thus set 1 Crab¹ as the typical limit between the off-flare and flaring intervals. We identify 18 main events, i.e. peaks that reached at least 6 Crab (labeled with Roman numerals² in Fig. 1, their main characteristics are given in the online table 1), with 11 exceeding 20 Crab during

¹ The ISGRI/20–40 keV CR of the Crab is 165 cts/s $\Leftrightarrow F_{20-40\text{keV}} = 8 \cdot 10^{-9}$ erg/cm²/s for a power law spectrum with $\Gamma=2.1$ and a normalization of 10 ph/cm²/s at 1 keV.

² V and XII contain two distinct events hardly distinguishable in Fig. 1. They appear under the same label in Fig. 1 (to keep it clear), and are named with a/b sub-labels in the text and table 1.

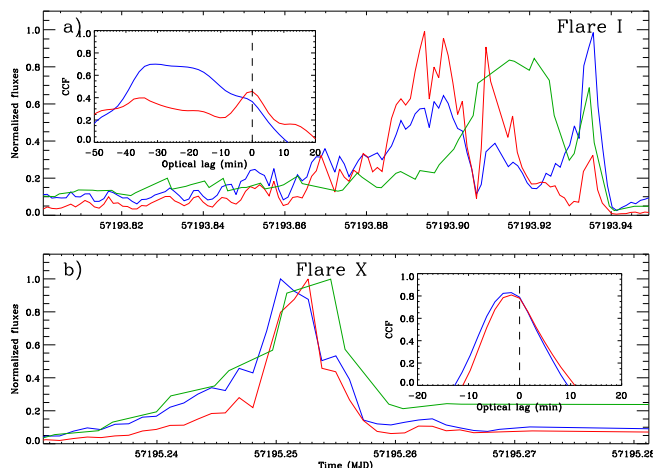


Fig. 2. V-band (green), 3–13 keV (red), and 20–40 keV (blue) LCs around flares I (a) and X (b). The inserts show the cross-correlation functions of the 3–13 keV (red) and 20–40 keV (blue) vs the optical LCs over the same time intervals as the LCs. The dashed vertical lines represent the 0 lag level.

our observations. Flares IV, XI, and XIII are the brightest we observed, reaching 43 Crab. The flares occur isolated (e.g. III, IV, VI) as well as in groups with peak to peak intervals as short as 22 min (Va, Vb). The flares last 0.4–2.4 hr except peaks IV and XIII. The former shows a rather broad profile and has multiple peaks. This event lasted 4.8 hr in total and it is the longest flare of our observation. The latter reached about 40 Crab. The peak itself lasted about 1.5 hr, but was preceded by a ~ 3 hr long, 3 Crab plateau seen only above 13 keV. It was followed by flares XIV and XV which show decreasing peak values.

The 3–13/20–40 keV softness ratio (SR, Fig. 1, right) shows that the large variability of the source is associated with variations of SR from ~ 0.03 to ~ 1.3 corresponding to $\Gamma=0.1$ – 2.5 in simulated JEM-X/ISGRI power law spectra. $SR \sim 0.6$ corresponds to $\Gamma=2.0$. Large spectral variations are visible in the off-flare intervals (Fig. 1, right). All the flares are hard, and they even all have $SR < 0.4$ ($\Leftrightarrow \Gamma < 1.8$).

4. Optical vs. X-ray behavior

The comparison of the optical (OMC) and X-ray (JEM-X1 and ISGRI) LCs shows a non trivial relationship. Significant flaring activity is evident in the V band LC (Fig. 1, left), with at least 12 clear flares. The optical flare typically last 0.24–2.5 hr. While some events occur in simultaneity with X-ray flares, the optical emission is delayed with respect to the X-rays in other cases. Fig. 2 shows typical examples of these different behaviors. The cross-correlation function (ccf) between the X-ray and optical emission confirms the absence of lags for some of the flares (e.g. flare I that causes the peak at 0 in the ccf of Fig. 2a), and delayed optical emission from 1.5 min to 20–30 min is seen in others. The ccf of Fig. 2b shows an example of a ~ 3 min lag, while the ccf of Fig. 2a (in addition to showing the simultaneity of peak I and its optical counterpart) shows lag at 20–30 min representing the delay between the small X-ray flares preceding peak I (around MJD 53193.9) and the subsequent optical flare (around MJD 53193.92). Due to the time resolution of OMC, however, lags shorter than 1 min can not be measured with our data, and additional lags of the order of seconds are not excluded.

While most of the flares show a fast rise similar to the flares

observed in X-rays, the two optical events occurring close to X-ray peaks IV and XIII seem to be exceptional. All other flares show fast rises (≤ 1 hr), but these two events have slower rises (about 10 and 4 hr, respectively), and are both coincident with hard plateaus that precede the X-ray peaks.

5. Spectral analysis

We accumulated spectra from the brightest flares ($CR > 1000$ cts/s) and the off-flare intervals ($CR < 165$ cts/s). In the latter case we also only retained the hard intervals ($SR < 0.6$) in order to exclude the softening visible after MJD 57197.9 (Fig. 1). The resultant “ ν - f_ν ” spectra are plotted in Fig. 3.

The off-flare spectrum is well fitted ($\chi^2_\nu=1.2$, 66 degrees of freedom, dof) by a model consisting of a power law with a high-energy cut-off dominating at 10–100 keV plus an additional power law dominating above 100 keV. The former component has $\Gamma=1.0^{+0.3}_{-0.4}$, $E_{\text{cut}}=16^{+4}_{-2}$ keV, $E_{\text{fold}}=23 \pm 5$ keV, the latter has $\Gamma=1.9^{+0.2}_{-0.3}$, (Γ is the photon index defined as $N(E) \propto E^{-\Gamma}$.) Normalization constants were included to account for potential cross-calibration issues, or differences in the effective exposures (deadtime corrections, telemetry drop out). When set to 1 for ISGRI, we get ~ 1.9 for SPI and ~ 0.6 for JEM-X1. The 20–400 keV (ISGRI) flux is $\sim 10^{-8}$ erg/cm²/s, and the above model leads to an extrapolated 0.1– 10^5 keV flux $\sim 3.8 \cdot 10^{-8}$ erg/cm²/s, i.e. about 2% L_{Edd} for a $9 M_\odot$ BH.

The flare spectrum is well represented ($\chi^2_\nu \sim 0.9$, 78 dof) by a single cut-off power law with $\Gamma=1.54 \pm 0.06$, $E_{\text{cut}}=14.0^{+2.8}_{-3.3}$ keV, $E_{\text{fold}}=87^{+4}_{-5}$ keV. An extra power law component is not statistically required according to an F-test. The normalization constants are both close to 1.1. The 20–400 keV (ISGRI) flux is $\sim 10^{-7}$ erg/cm²/s, which leads to an extrapolated 0.1– 10^5 keV flux $\sim 3 \cdot 10^{-7}$ erg/cm²/s, i.e. about 20% L_{Edd} for a $9 M_\odot$ BH.

6. Discussion

Over the 4 days covered by our *INTEGRAL* ToO, V404 showed a high level of emission with sporadic flares with a maximum 20–40 keV dynamical range of 940 (flare XVI). During its flares V404 became the brightest X-ray object in the sky. In the hard off-flare state the spectral analysis shows the presence of two spectral components: a cut-off power law usually attributed to thermal Comptonization and an extra power law at energies beyond 100 keV. Hard tails have now been seen in a large number of systems (e.g. GRS 1915+105, Swift J1753.5–0127, GX 339–4, or Cyg X-1, Rodríguez et al. 2008b; Tomsick et al. 2015; Joinet et al. 2007; Rodríguez et al. 2015b) and their origin is still highly debated, although a compact jet origin is favored in the case of Cyg X-1 (e.g. Russell & Shahbaz 2014; Rodríguez et al. 2015b). It is interesting to remark that the flaring activity seems primarily due to spectral variations of the cut-off power law only. We estimate an integrated luminosity $L \sim 0.2 L_{\text{Edd}}$ for the >6 Crab flares. This is a lower limit to the maximum luminosity reached at the peak of the brightest flares. First because we averaged the data, without isolating the brightest portions of the flares. Also we did not consider all the contributions below 10 keV (disk, jet) that can provide a significant fraction of the bolometric luminosity. Assuming a simple scaling between the CR and L_{Edd} with a constant shape for the variable component between the off-flare hard state and the flares, we conclude that all peaks with $CR \geq 3000$ cts/s (~ 18 Crab) (flares III, IV, Va, b, VIII, X, XI, XIIIa, b, XIII and XIV, Fig. 1) reached $\sim L_{\text{Edd}}$.

The optical activity is also highly variable and shows flares

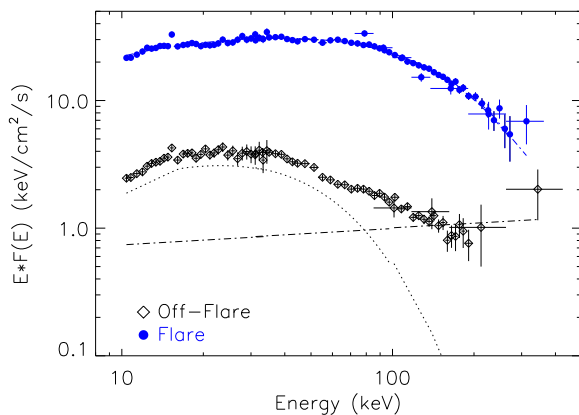


Fig. 3. ν - f_ν spectra obtained from the fits to the off-flare and flare intervals. The lines represent the spectral components used for the fits.

(Fig. 1, 2). Some optical flares occur in conjunction with the X-rays, while other activity periods show delays (Fig. 2). The first specific length scale of this system is the separation between the BH and the companion: using the system parameters from Sec. 1 and a $9 M_\odot$ BH we estimate $\sim 2.2 \cdot 10^{12}$ cm or ~ 75 light seconds. Hence, when no delay between the optical and the X-rays is observed (e.g. flare I in Fig. 2a), the mechanism producing the optical emission could be related to X-ray reprocessing, either by an accretion disk or by the companion. The maximum delays expected would be around 60 s (outer disk), and $\lesssim 150$ s (companion located at superior conjunction).

Optical lags ≥ 10 min could be related to variable jet properties, either as their intrinsic synchrotron emission, or from their interaction with the surrounding medium. Radio, and millimeter (mm) flaring activity ascribed to discrete ejections have been reported during this outburst (e.g. Sivakoff et al. 2015; Mooley et al. 2015; Tetarenko et al. 2015b). Delays between X-rays and longer wavelengths are expected in the case of adiabatically expanding ejecta (van der Laan 1966; Mirabel et al. 1998), and we remark that Tetarenko et al. (2015b) report a mm peak on MJD 57195.548, about 26 min after the MJD 57195.53 X-ray event (a < 6 Crab flare that occurred slightly after flare XII). Interestingly, this delay also corresponds to the timescale of the mm flare increase (Tetarenko et al. 2015b) which renders the mm compatible with being causally related to the X-ray flare. As in other well known sources, e.g. XTE J1550–564, GRO J1655–40, GRS 1915+105 (Fender 2006), in V404 discrete ejections may be causally connected to the X-ray activity.

V404 reached maximum absolute peak intensities that are rather usual during outbursts of microquasars. If V404 was at 10 kpc the maximum peak intensity would have been 2.5 Crab, a value similar to the aforementioned other microquasars during their brightest outburst(s) (e.g. Remillard & McClintock 2006). Short recurrent (multi-wavelength) flares have, however, been seen only in GRS 1915+105 (e.g. Greiner et al. 1996), and in V404 the flaring activity similarly recurs on timescales as short as 22 min. Some of the V404 optical flares lag ≥ 20 minutes behind the X-rays (Fig. 2a), and similar lags are also seen at mm-radio wavelengths. This may resemble the correlated X-ray/infrared/radio oscillations also referred to as “30-minutes” cycles of GRS 1915+105 (e.g. Fender & Pooley 1998; Mirabel et al. 1998; Rodriguez et al. 2008a). In GRS 1915+105, however, these events are associated with hard X-ray dips preceding the flares and a clear softening at the X-ray peak, marking

the disappearance of the Comptonization component (Rodriguez et al. 2008b). V404, on the contrary, remains hard even in the flaring states (Fig. 1), indicating a different mechanism responsible for the X-ray flaring (similar results were obtained from the 1989 outburst, e.g. Życki et al. 1999). One tempting possibility would be that the high-energy flares are direct boosted emission from a jet (blazar-like configuration). This would imply a jet axis not perpendicular to the orbital plane. Misaligned jets have been seen in GRO J1655–40 and V4641 Sgr (Maccarone 2002, and references therein). In the former, a rather modest Lorentz factor $\gamma \sim 2.5$ implies small relativistic boosting (Hjellming & Rupen 1995). In the latter, γ ranges from 10 up to 17, and the angle between the jet axis and the orbital plane normal is as high as 50° (Maccarone 2002, and references therein). Significant Doppler boosting is expected in this case.

Życki et al. (1999) argued that the spectral and intensity variability seen with Ginga in 1989 could be due to the evolution of a heavily absorbing medium. However, even with $N_H \gtrsim 10^{24}$ cm $^{-2}$ (Życki et al. 1999), the activity above 20 keV is not affected by absorption, and hence the absorber alone cannot be responsible for the large variability we observe. The high energy flares could be due to the shock of the relativistic jets with the dense ambient medium. Then optically thin synchrotron emission would be expected at X-ray energies, while our analysis favors thermal Comptonization. More simultaneous multi-wavelength observations will help disentangling these different possibilities.

Acknowledgements. We warmly thank the referee for his/her useful report that helped us to improve the quality of this paper. We also thank the *INTEGRAL* teams and planners for their prompt reaction and the scheduling of these observations. JR, MC, SC acknowledge funding support from the French Research National Agency: CHAOS project ANR-12-BS05-0009 (<http://www.chaos-project.fr>), and from the UnivEarthS Labex program of Sorbonne Paris Cité (ANR-10-LABX-0023 and ANR-11-IDEX-0005-02). XLZ acknowledges funding through DLR 50 OG 1101. MGHK was supported by the Deutsche Forschungsgemeinschaft under DFG project number PR 569/10-1 in the context of the Priority Program 1573 Physics of the Interstellar Medium. This work was supported by NASA through the Smithsonian Astrophysical Observatory (SAO) contract SV3-73016 for the Chandra X-Ray Center and Science Instruments. RD and XLZ acknowledge support through the Deutsches Zentrum für Luft- und Raumfahrt e.V. (DLR) 50 OG 1101. OMC activities are supported by Spanish MINECO grant ESP2014-59789-P. This study is based on observations made with *INTEGRAL*, an ESA project with instruments and science data centre funded by ESA member states, Poland and with the participation of Russia and the USA.

References

- Barthelmy, S. D., D’Ai, A., D’Avanzo, P., et al. 2015, GCN, 17929, 1
 Casares, J. & Charles, P. A. 1994, in AIP Conference Series, Vol. 308, The Evolution of X-ray Binaries, ed. S. Holt & C. S. Day, 107
 Casares, J., Charles, P. A., & Naylor, T. 1992, Nature, 355, 614
 Corbel, S., Koerding, E., & Kaaret, P. 2008, MNRAS, 389, 1697
 Domingo, A., et al. 2015, The Astronomer’s Telegram, 7717, 1
 Fender, R. 2006, in Compact stellar X-ray sources, 381–419
 Fender, R. P. & Pooley, G. G. 1998, MNRAS, 300, 573
 Ferrigno, C., Fotopoulou, S., Domingo, A., et al. 2015, ATel, 7662, 1
 Greiner, J., Morgan, E. H., & Remillard, R. A. 1996, ApJ, 473, L107
 Hjellming, R. M. & Rupen, M. P. 1995, Nature, 375, 464
 Hynes, R. I., Charles, P. A., Garcia, M. R., et al. 2004, ApJ, 611, L125
 Jinet, A., Jourdain, E., Malzac, J., et al. 2007, ApJ, 657, 400
 Khargharia, J., Froning, C. S., & Robinson, E. L. 2010, ApJ, 716, 1105
 Kuulkers, E., Motta, S., Kajava, J., et al. 2015, ATel, 7647, 1
 Maccarone, T. J. 2002, MNRAS, 336, 1371
 Makino, F., Wagner, R. M., Starrfield, S., et al. 1989, IAU Circ., 4786, 1
 Miller-Jones, J. C. A., Jonker, P. G., Dhawan, V., et al. 2009, ApJ, 706, L230
 Mirabel, I. F., Dhawan, V., Chaty, S., et al. 1998, A&A, 330, L9
 Mooley, K., Fender, R., Anderson, G., et al. 2015, ATel, 7658, 1
 Motta, S., Beardmore, A., Oates, S., et al. 2015, ATel, 7666, 1
 Munoz-Darias, T., Sanchez, D. M., Casares, J., et al. 2015, ATel, 7659, 1
 Negoro, H., Matsumitsu, T., Mihara, T., et al. 2015, ATel, 7646, 1
 Remillard, R. A. & McClintock, J. E. 2006, ARA&A, 44, 49

- Richter, G. A. 1989, *Information Bulletin on Variable Stars*, 3362, 1
- Rodriguez, J., Ferrigno, C., Cadolle Bel, M., et al. 2015a, *ATel*, 7702, 1
- Rodriguez, J., Grinberg, V., Laurent, P., et al. 2015b, *ApJ*, 807, 17
- Rodriguez, J., Hannikainen, D. C., Shaw, S. E., et al. 2008a, *ApJ*, 675, 1436
- Rodriguez, J., Shaw, S. E., Hannikainen, D. C., et al. 2008b, *ApJ*, 675, 1449
- Russell, D. M. & Shahbaz, T. 2014, *MNRAS*, 438, 2083
- Shahbaz, T., Ringwald, F. A., Bunn, J. C., et al. 1994, *MNRAS*, 271, L10
- Sivakoff, G. R., Tetarenko, A., & Miller-Jones, J. C. 2015, *ATel*, 7671, 1
- Strong, A. W., Diehl, R., Halloin, H., et al. 2005, *A&A*, 444, 495
- Terada, K., Miyamoto, S., Kitamoto, S., & Egoshi, W. 1994, *PASJ*, 46, 677
- Tetarenko, A., Sivakoff, G. R., Gurwell, M. A., et al. 2015a, *ATel*, 7661, 1
- Tetarenko, A., et al. 2015b, *ATel*, 7708, 1
- Tomsick, J. A., Rahoui, F., Kolehmainen, M., et al. 2015, *ApJ*, 808, 85
- Tsubono, K., Aoki, T., Asuma, K., et al. 2015, *ATel*, 7701, 1
- van der Laan, H. 1966, *Nature*, 211, 1131
- Winkler, C., Courvoisier, T. J.-L., Di Cocco, G., et al. 2003, *A&A*, 411, L1
- Xie, F.-G., Yang, Q.-X., & Ma, R. 2014, *MNRAS*, 442, L110
- Życki, P. T., Done, C., & Smith, D. A. 1999, *MNRAS*, 309, 561

Table 1. List of the >6 Crab flares and their main properties. MJD 57193 is 2015 June 20th.

Name	Start ^a (MJD)	Peak time (MJD)	Stop ^a (MJD)	CR _{3–13 keV} ^b (cts/s)	CR _{20–40 keV} ^b (cts/s)	Properties ^c
I	57193.9217	57193.9356	57193.9402	184	1215	Multiple
II	57193.9703	57193.9981	57194.0827	181	1234	Multiple
III	57194.0827	57194.1152	57194.1428	1055	5209	Complex
IV	57194.2232	57194.3107	57194.3938	2010	7040	Isolated/Complex
Va ^d	57194.6273	57194.6399	57194.6521	473 ^e	3328	Multiple/Complex, preceded by plateau
Vb ^d	57194.6521	57194.6579	57194.6708	852	3999	Multiple/Complex
VI	57194.6960	57194.7346	57194.7473	129	1974	Isolated/Complex
VII	57194.9788	57194.9996	57195.0089	459	2200	Multiple/Complex
VIII	57195.0089	57195.0293	57195.0501	865	4950	Multiple/Complex
IX	57195.0582	57195.0826	57195.1095	320	2386	Multiple/Complex
X	57195.2318	57195.2503	57195.2712 ^f	577 ^g	3472	Multiple, preceded by succession of ~6 Crab peaks
XI	57195.4294	57195.4388	57195.4450	857	7036	Multiple
XIIa ^d	57195.4450	57195.4573	57195.4665	401	3525	Multiple/Complex
XIIb ^d	57195.4665	57195.4723	57195.4841	1231	6299	Multiple, followed by plateau
XIII	57197.1373	57197.1785	57197.1924	2076	7081	Multiple, preceded by plateau
XIV	57197.1924	57197.2020	57197.2067	1240	4368	Multiple
XV	57197.2124	57197.2228	57197.2310	210	1793	Multiple/Complex
XVI	57197.3450	57197.3647	57197.3705	151	1036	Isolated

^a Start (resp. stop) time of a flare is defined as the time 20–40 keV CR reaches 165 cts/s (1 Crab) during the increase (resp. decrease), or by the minimum reached before (resp. after) the increase (decrease) for multiple flares. The uncertainty on the times is $\pm 6 \times 10^{-4}$ d.

^b Count rates at the peaks

^c “Multiple” stands for series of well defined flares occurring in rapid repetition. “Complex” stands for flares showing various peaks. “Plateau” indicates a >1 Crab plateau.

^d These peaks appear as single peaks in Fig. 1. They are in fact true multiples.

^e The 3–13 keV peak time occurred about 200 s before the 20–40 keV one, indicating a potential hard lag.

^f Data gap at the end of the flare. The stop time is the last point before the gap.

^g The 3–13 keV peak time occurred about 200 s after the 20–40 keV one, indicating a potential soft lag.

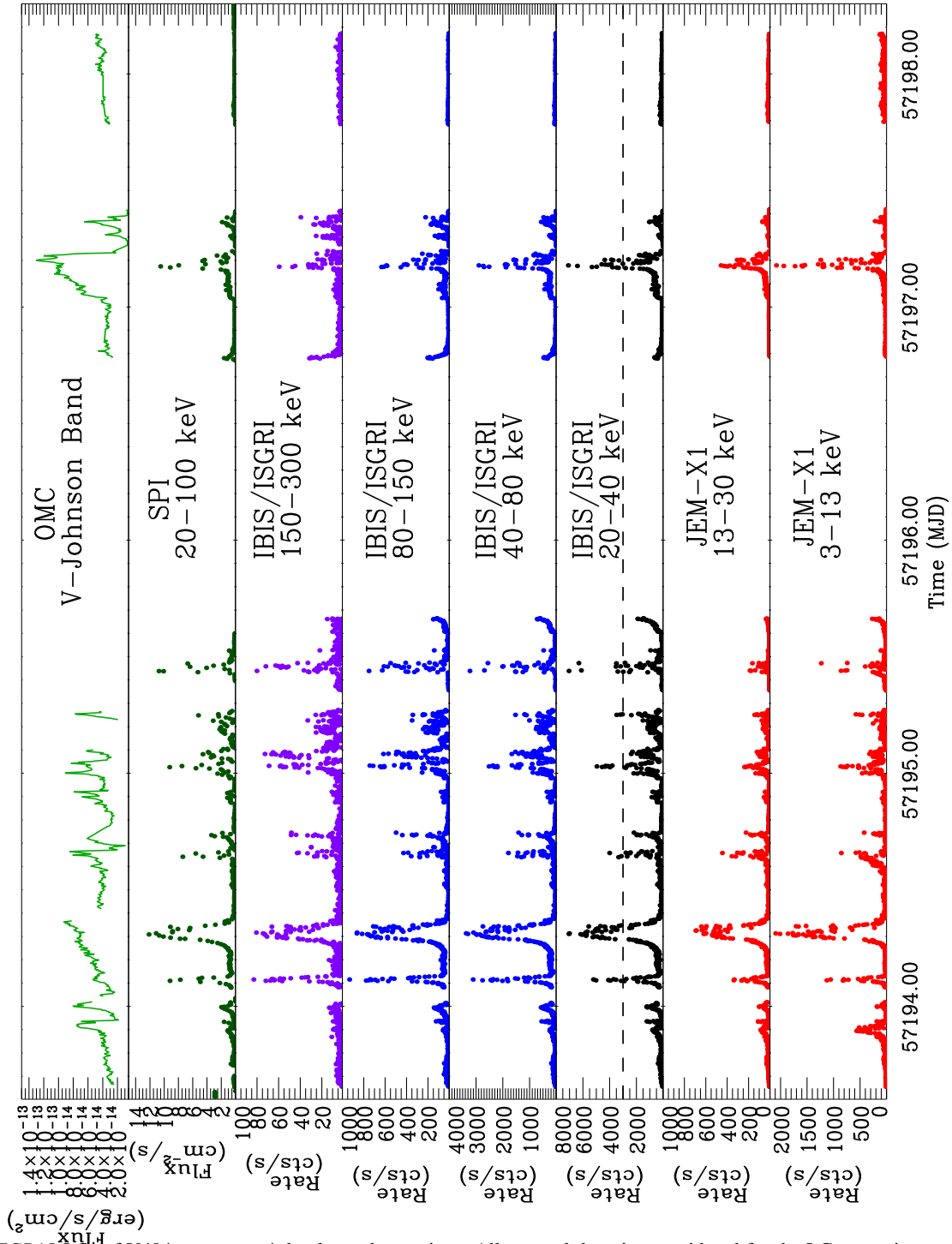


Fig. 4. *INTEGRAL* LCs of V404 over our ~4 day-long observations. All spectral domains considered for the LC extraction are shown here. The dashed line in the 20–40 keV panel represents the approximate level of L_{Edd} we estimated. MJD 57193 is 2015 June 20th.